

Article

Not peer-reviewed version

Numerical Simulation of the Effect of Pre-Strain on Fatigue Crack Growth in AA2024-T351

[Diogo M. Neto](#) , [Edmundo Sérgio](#) , André Agra , [Fernando V. Antunes](#) *

Posted Date: 1 April 2025

doi: 10.20944/preprints202504.0004.v1

Keywords: fatigue crack growth; AA2024-T351; pre-strain; crack closure; CTOD



Preprints.org is a free multidisciplinary platform providing preprint service that is dedicated to making early versions of research outputs permanently available and citable. Preprints posted at Preprints.org appear in Web of Science, Crossref, Google Scholar, Scilit, Europe PMC.

Copyright: This open access article is published under a Creative Commons CC BY 4.0 license, which permit the free download, distribution, and reuse, provided that the author and preprint are cited in any reuse.

Article

Numerical Simulation of the Effect of Pre-Strain on Fatigue Crack Growth in AA2024-T351

Diogo M Neto, Edmundo Sérgio, André Agra [†] and Fernando V Antunes ^{*}

University of Coimbra, ARISE, CEMMPRE, Department of Mechanical Engineering, 3030-788 Coimbra, Portugal

^{*} Correspondence: fernando.ventura@dem.uc.pt

[†] Current address: Aptiv, R. Max Grundig, 4705-086 Braga, Portugal.

Abstract: The objective here is to study the effect of pre-strain on fatigue crack growth (FCG) in 2024-T351 aluminium alloy. Three pre-strain conditions were considered: without pre-strain, compressive and tensile permanent pre-strains of 4%. A numerical approach based on cumulative plastic strain at the crack tip was followed to predict FCG rate. The compressive pre-strain increased FCG rate, while the tensile pre-strain reduced the da/dN relatively to the situation without pre-strain. The influence of pre-strain was linked with plasticity induced crack closure. In fact, a linear trend was obtained between da/dN and ΔK_{eff} for three crack lengths ($a=16.184$; $a=15.048$ mm and $a=15.152$ mm) and three pre-strain conditions. The increase of stress ratio from $R=0.1$ to $R=0.5$ and the elimination of the contact of crack flanks reduced significantly the effect of pre-strain, also pointing for the huge relevance of crack closure in this context. Finally, the effect of pre-strain on da/dN after an overload was also explained by crack closure variations.

Keywords: fatigue crack growth; AA2024-T351; pre-strain; crack closure; CTOD

1. Introduction

Real structural components are submitted to plastic deformation during fabrication. Operations like blanking, trimming, stretching, bending and deep drawing are involved in structure fabrication. Sheet metal parts for automotive industry are produced by stamping [1], involving large plastic deformation. Material deformation can also be done to improve the mechanical properties, namely tensile strength and yield stress [2,3]. Plastic deformation resulting from fabrication affects material behaviour [4,5], so it must be included in the design of components and structures.

In laboratory testing or numerical simulation, the effect of pre-strain is studied loading a material up to the desired amount, so that it can experience deformation in the plastic strain regime, and then unload the material. The pre-strain increases the yield stress and tensile strength, while it decreases the ductility. In other words, the material becomes less ductile with pre-strain. This was observed by Ghosal et al. in dual-phase (DP590) steel [6,7], by Le et al. [8] in DP600 steel, by Fredriksson et al. [9] in DP400, DP600, HSLA steel (HSLA500) and a deep-drawing quality steel. Similar trends were also found by Wang et al. [10] for TWIP steel, Walker et al. [11] for DP and FB steels, Ji et al. [12] for different grades of DP steels, Wu et al. [13] for stainless steel (SUH660). These effects of pre-strain are explained by a substantial increase in dislocations [6], leading to localized alterations in lattice orientations. The increased dislocation density of the pre-strained material leads to significant work hardening.

In the high-cycle fatigue regime (HCF), fatigue strength can be defined as the specific stress amplitude below which a material can withstand an infinite number of cycles without failure. Ghosal et al. [6] and Le et al. [7] observed an increase of endurance limit with pre-strain in dual-phase steel. Wang et al. [10] studied AA2024-T3 and found a decrease in fatigue strength. Considering these opposite trends, the influence of tensile pre-strain on high-cycle fatigue life is expected to be material-

dependent. In fact, Froustey et al. [14] studied AA5454 and AA2017. The AA2017 showed a considerable reduction in fatigue life, but the AA5454 revealed unaffected fatigue properties with increasing the tensile pre-straining magnitudes.

The effect of pre-strain on low-cycle fatigue (LCF) has also been widely studied. Le Roux et al. [15] studied 304L stainless steel subjected to uniaxial pre-strain. They found a decrease in fatigue life compared to the as-received condition, under strain-controlled cycling, which was attributed to the reduction in ductility. Gustavsson et al. [16] studied dual-phase (DP) steel subjected to uniaxial pre-strain. They also observed a reduction in the fatigue life under fully reversed strain-controlled fatigue loading. Parker et al. [17] investigated the effect of 40% balanced biaxial stretching on hot rolled low carbon steel SAE1008. They reported that fatigue resistance starts to degrade in the LCF region compared to the as-received condition due to the cyclic softening nature of the stretched material. The pre-straining decreases ductility, which can cause poor fatigue performance in the LCF region. In contrast, it was found that fatigue resistance improves in the HCF region. The same trends were observed in DP600 steel submitted to 12.5% uniaxial pre-strain [18]. Rex et al. [19] studied the 2024-T4 aluminium alloy. A considerable increase in fatigue life was found for uniaxial tensile pre-strained in comparison to the 0% prestrained condition at higher strain amplitude. Furthermore, equi-biaxial tensile pre-strained specimens showed a quite small increment in fatigue life compared to 0% pre-strained material. As-received specimens exhibit noticeable cyclic hardening at all the strain amplitude values. The pre-strained specimen shows an almost stable cyclic stress-strain response for each strain amplitude. Branco et al. [20] studied the effect of 4 and 8% tensile pre-strains on the LCF in AA7050-T6. They observed a reduction of fatigue life with pre-strain. Without pre-strain the dislocations tended to have a more homogeneous distribution, while under higher tensile pre-strains, the dislocations were mainly observed at the slip bands.

The effect on fatigue crack growth (FCG) has also been studied. Schijve [21] studied aluminium alloys and observed a substantial rise in FCG rate of 2024-T3 alloy after applying a 3% tensile pre-strain. He suggested that the elevated yield strength due to pre-straining leads to a smaller plastic zone size, intensifying tensile stresses and diminishing crack closure within the plastic zone near the crack tip, thereby accelerating crack propagation. Al-Rubaie et al. [22] studied AA7475-T7351 and found a limited effect of pre-straining in regimes I and II, but an effect in regime III associated with a loss of fracture toughness. Anandavijayan et al. [23] also found a limited effect in S355 steel submitted to pre-strains of 0, 5 and 10%. On the contrary, they found a great influence on high-cycle fatigue life. Tai Shan and Liu [24] observed an increase of FCG rate in AA2024-T351. Wasen et al. [25] found that pre-straining reduces FCG rate in dual-phase steel. Arora et al. [26] studied mild steel and observed a decrease of FCG rate in regime II. Radhakrishnan et al. [27] investigated the influence of pre-straining and stress ratio on FCG in mild and stainless steel. They observed that the FCG rate decreased by factors of 2.4 and 3.7 for 6% and 9% pre-strains and 1.4 and 2.4 for 9% and 14% pre-strains in mild and stainless steel, respectively. In contrast to earlier findings, Kim et al. [28] showed that FCG rate increases with higher pre-strain levels in the lower and intermediate ΔK regimes in PH steel. Leitner et al. [29] also found that increased plastic pre-deformation increases the FCG rate and ΔK_{th} in pearlitic steel. The conclusions from the above literature demonstrate that the influence of plastic pre-strain on FCG response is greatly dependent on material. However, there is a lack of understanding of the mechanisms explaining the effect of pre-strain. Besides, the effect of compressive pre-strain on FCG has not been reported.

The objective of this research is to study the effect of pre-strain on FCG in 2024-T351 aluminium alloy. A numerical model was built to simulate the application of pre-strain and the subsequent propagation of a fatigue crack by node release. Tensile and compressive pre-strains of 4% were studied.

2. Numerical model

Figure 1a shows the CT specimens considered in the numerical study. These specimens had a width $W=36$ mm and an initial crack length $a_0=15$ mm. Only 1/4 of CT specimen was modelled, as

indicated in Figures 1b and 1c, considering adequate boundary conditions. The cyclic load was applied in the upper point of the specimen hole, considering a nodal force. Rigid body movement is inhibited fixing the lower right corner, as indicated in Figure 1b. The contact of crack flanks was simulated using a rigid plane placed at the crack symmetry plane. A small thickness of 0.1 mm was considered for the specimen, in order to model a plane stress state. Simulations without contact between crack flanks were also run, to understand the effect of crack closure.

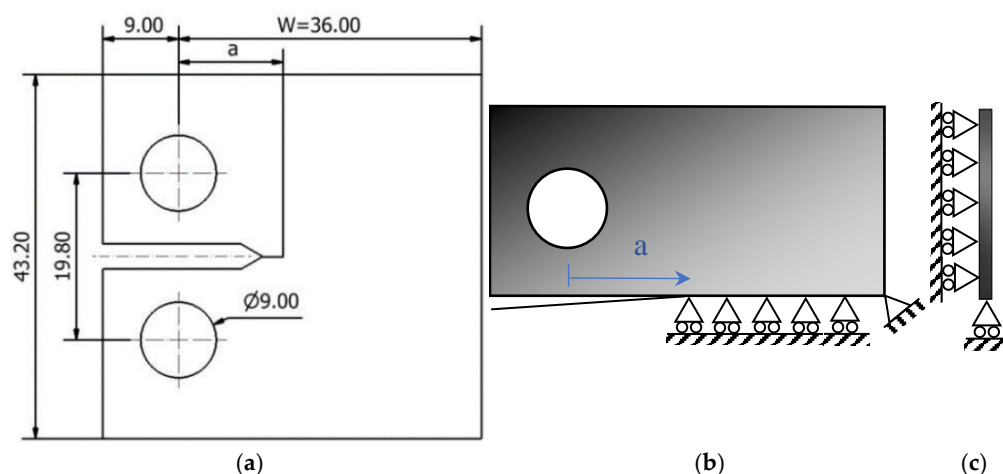


Figure 1. (a) Geometry of CT specimen (dimensions in mm). (b) (c) Physical model.

The material studied was the 2024-T351 aluminium alloy. The 2XXX series of aluminium alloys are widely used in aerospace applications owing to their high strength, good fracture toughness, and low density [30]. As a result of its high strength-to-weight ratio, the Al–Cu–Mg–Mn based AA2024 aluminium alloy is widely used for various engineering applications, including aircraft and transportation applications [31,32]. Typically, this material is used in the design of fuselage, wings, and lightweight components in the aerospace industry. Table 1 shows the chemical composition of the 2024-T351 aluminium alloy used in this research. The material properties of the 2024-T351 aluminium alloy without pre-strain, determined with a tensile test, are: Young modulus=73 GPa, Yield stress=325 MPa, Ultimate Tensile Strength (UTS)=470 MPa, Elongation at break=20% and Brinell Hardness=137.

Table 1. Chemical composition in weight % of 2024-T351 aluminium alloy. The balance is Al.

Si	Fe	Cu	Mn	Mg	Cr	Zn	Ti
0.50	0.50	3.8-4.9	0.3-0.9	1.2-1.8	0.10	0.25	0.15

The accurate modelling of material elastic-plastic behaviour is fundamental to obtain good quality numerical predictions of crack tip plastic deformation. The elastic behaviour is assumed isotropic and described by Hooke's law. On the other hand, the plastic behaviour is characterised by the von Mises yield criterion and the Swift isotropic hardening law coupled with Lemaître-Chaboche kinematic hardening law under an associated flow rule. Swift hardening law [33] is described by:

$$Y=C \left[\left(\frac{Y_0}{C} \right)^{\frac{1}{n}} + \bar{\epsilon}^P \right]^n \quad (1)$$

where Y_0 , C and n are the material parameters and $\bar{\epsilon}^P$ denotes the equivalent plastic strain. The Lemaître-Chaboche kinematic hardening law [34] is:

$$\dot{\mathbf{X}}=C_x \left[X_{Sat} \frac{\sigma'-\mathbf{X}}{\bar{\sigma}} - \mathbf{X} \right] \dot{\bar{\epsilon}}^P \quad (2)$$

where C_x and X_{Sat} are the material parameters of Lemaître-Chaboche law, $\bar{\sigma}$ is the equivalent stress and $\dot{\epsilon}^p$ is the equivalent plastic strain rate. The material parameters, presented in Table 2, were identified using LCF fatigue curves obtained for $R_\epsilon = -1$ and $\Delta\epsilon/2 = 1.5\%$ in a previous research [35].

Table 2. List of material parameters involved in the Swift and Lemaître-Chaboche laws.

Material	Y_0 [MPa]	C [N]	n	C_x [mm]	X_{Sat} [MPa]
2024-T351	288.96	389.00	0.056	138.80	111.84

The numerical model was implemented using the in-house software DD3IMP (Three-Dimensional Elasto-Plastic Finite Element Code), originally developed for the simulation of deep-drawing [36]. An updated Lagrangian approach is used to describe the evolution of the deformation process, assuming a hypoelastic-plastic model. The numerical model considers large elastoplastic strains and rotations, while the elastic strains are assumed negligibly small. Figure 2 shows the finite element mesh considered, where the specimen was discretized with linear 8-node hexahedral finite elements, using a selective reduced integration technique to avoid volumetric locking. It was refined in the crack growth region, having elements with $8 \times 8 \mu m^2$. In regions relatively distant from the propagation zone finite elements have larger dimensions, in order to reduce the total number of elements and thus the numerical effort. Only one layer of elements was considered along the thickness direction. The model comprises 14625 finite elements and 29756 nodes.

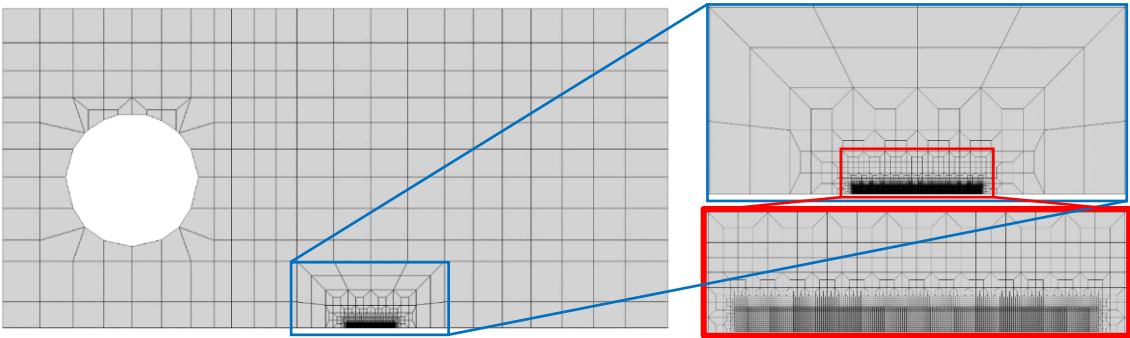


Figure 2. Finite element mesh.

Crack propagation was numerically modelled by successive debonding of both current crack front nodes. This crack propagation is fundamental to generate a residual plastic and therefore to stabilize the crack closure level. The release occurs at minimum load to avoid convergence problems that may arise due to crack propagation at maximum load. The size of each crack increment corresponded to the finite element size in the refined region. The two crack front nodes were released when the accumulation of plastic strain reached the critical value of strain. This critical value was calibrated using one experimental value of da/dN , and a value of 110% was obtained in a previous study of the authors [37].

The pre-strain was applied by displacing a range of nodes along the entire width of the specimen. This displacement simulated what would experimentally be a distributed tensile or compressive load on the specimen. The region where plastic deformation was induced is indicated by the red rectangle in Figure 3. The region above it is free from pre-deformation. The displacements were adjusted to obtain plastic deformations of 4% in tension and compression ($\epsilon_{ps} = -4, +4\%$). After the application of pre-deformation, a crack with a length $a_0 = 15$ mm was simulated and submitted to cyclic loading and crack propagation by node release.

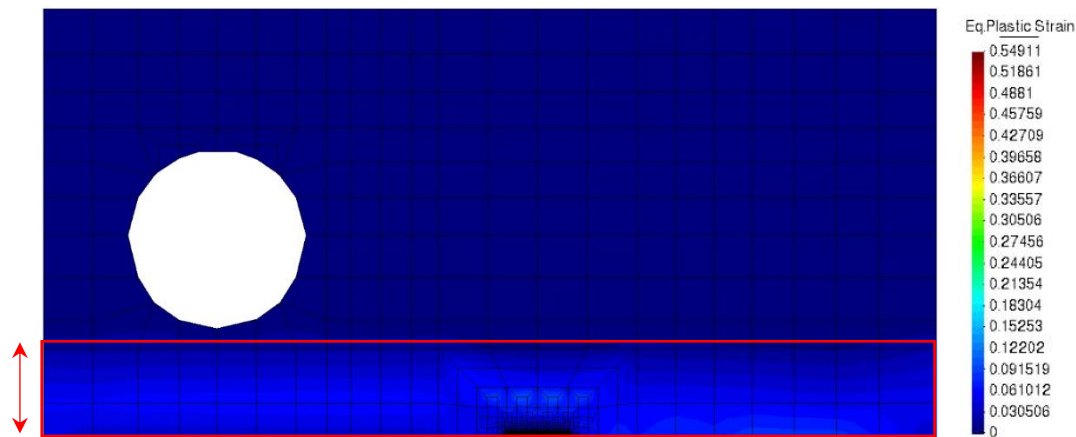


Figure 3. Geometry of CT specimen (dimensions in mm). (b) Physical model.

The CT specimen was submitted to constant amplitude loading with stress ratios $R=0.1$ and $R=0.5$. In the first case, the maximum and minimum forces were 41.67 N e 4.17 N, being 75 N and 37.5 N for a stress ratio $R=0.5$. Simulations of overloads were also considered. In the overload cycle the maximum and minimum loads were 79.17 N and 4.17, respectively, giving an overload ratio $OLR=1.5$, calculated according:

$$OLR = \frac{F_{OL} - F_{min}}{F_{max} - F_{min}} \quad (3)$$

The baseline loading had $F_{max}=41.67$ N and $F_{min}= 4.17$ N, respectively. Table 3 presents all the load cases considered. Simulations without contact of crack flanks were also considered, as already mentioned.

Table 3. Loading conditions ($a_0=15$ mm; plane stress).

Test	Loading	R	ϵ_{ps} [%]	Contact
1	CA	0.1	0	Yes
2	CA	0.1	+4	Yes
3	CA	0.1	-4	Yes
4	CA	0.1	0	No
5	CA	0.1	+4	No
6	CA	0.1	-4	No
7	CA	0.5	0	Yes
8	CA	0.5	+4	Yes
9	CA	0.5	-4	Yes
10	OL	0.1 (BL) ¹	0	Yes
11	OL	0.1 (BL)	+4	Yes

¹ BL- Baseline loading.

3. Results

3.1. Effect of Pre-Strain on da/dN

Figure 4 shows the variation of FCG rate versus crack length, a , with and without pre-strain. The crack propagation started at $a_0=15$ mm and ended at $a=16.2$ mm. This propagation is enough to stabilize the level of plastic induced crack closure.

The specimen without pre-strain presents an initial small increase of da/dN , followed by a progressive decrease to a minimum value, which occurs at about $a=15.5$ mm. This decrease is

explained by the progressive increase of crack closure level with the formation of residual plastic wake. Above this transient regime there is a stable regime characterised by a progressive increase of da/dN , which is explained by the increase of crack tip fields with crack length.

The specimen with a tensile pre-strain of 4% presents a similar behaviour, but the variations are much smaller. There is a small increase of da/dN , followed by a smooth decrease to a minimum value which occurs at about $a=15.2$ mm. Finally, there is a progressive increase with crack propagation as a result of the increase of crack length.

The specimen submitted to a compressive pre-strain of 4% presents a small initial increase of da/dN , but without subsequent decrease. The slope of increase of da/dN with crack length is similar to that observed for the specimen without pre-strain. On the other hand, the specimen with tensile pre-strain has a lower rate of variation of da/dN in the stable regime. The FCG rate in the stable regime is higher for the compressive pre-strain, intermediate for the specimen without pre-strain, and lower for the tensile pre-strain. For a crack length of 16.184 mm, indicated by the vertical dashed line, da/dN has values of 0.95, 0.71 and 0.39 $\mu\text{m}/\text{cycle}$ for $\varepsilon_{ps}=-4$, 0 and +4%, respectively.

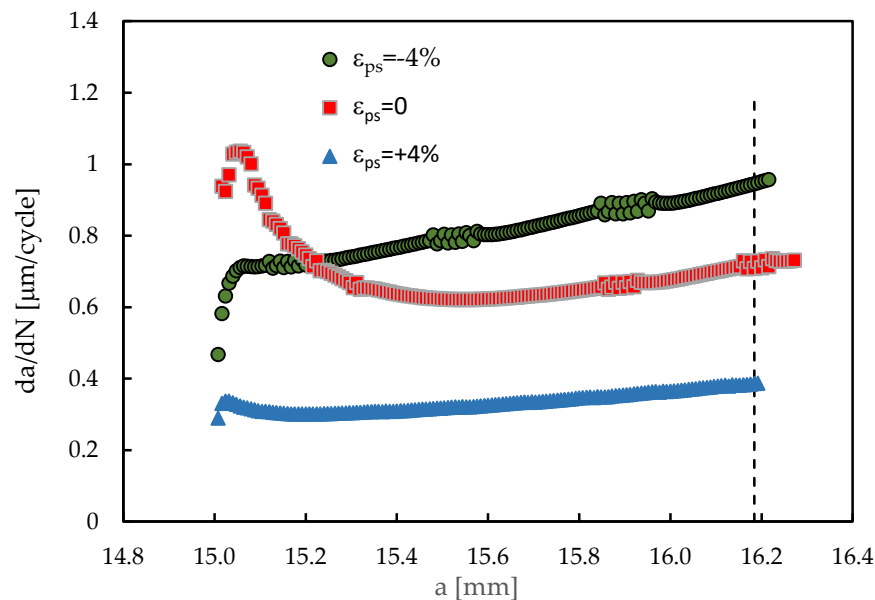


Figure 4. Effect of pre-strain on FCG (Plane stress; $R=0.1$; $F_{\min}=4.17$ N; $F_{\max}=41.67$ N; with contact).

Figure 5 presents the CTOD versus load plots, which are particularly interesting to understand what is happening at the crack tip. The CTOD curves plotted were measured at the first node behind crack tip for a crack length $a=16.184$ mm, indicated by the vertical dashed line on the right-hand side of Figure 4. The load ranged between $F_{\min}=4.17$ N and $F_{\max}=41.67$ N, as can be seen in the horizontal axis. The crack is closed at the lower part of the load cycle, having a linear elastic behaviour after opening. At relatively high loads there is a departure from linearity, resulting from crack tip plastic deformation. The elastic and plastic CTOD ranges (δ_e and δ_p , respectively), are indicated for the compressive pre-strain.

The crack opening level is lower for the compressive pre-strain ($F_{\text{open}} \approx 10$ N), and higher for the tensile pre-strain ($F_{\text{open}} \approx 20$ N), having an intermediate value for the specimen without pre-strain ($F_{\text{open}} \approx 15$ N). The crack opening level was quantified using:

$$U^* = \frac{F_{\max} - F_{\text{open}}}{F_{\max} - F_{\min}} \quad (1)$$

The compressive pre-strain has $U^*=18.23\%$, the situation without pre-strain has $U^*=27.15\%$, and the tensile pre-strain has $U^*=42.53\%$. The increase of crack opening level decreases the effective load range, which reduces maximum CTOD, the elastic and plastic deformation ranges and the area of the

loop (which is proportional of the dissipated energy). The sizes of monotonic plastic and reversed plastic zones are also expected to decrease. Therefore, a relation may be established between these non-linear parameters and da/dN values presented in Figure 4.

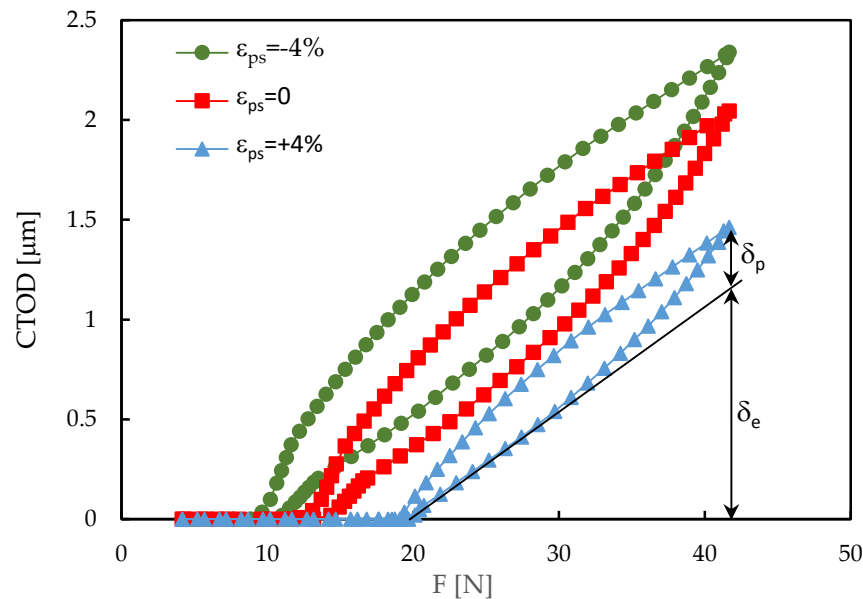


Figure 5. Variation of Crack tip Opening Displacement (CTOD) with applied load ($a=16.184$ mm; Plane stress; $R=0.1$; $F_{min}=4.17$ N; $F_{max}=41.67$ N; with contact).

The relation between FCG rate and the effective stress intensity factor range, ΔK_{eff} , was studied for three crack lengths ($a=16.184$; $a=15.048$ mm and $a=15.152$ mm) and three pre-strain conditions ($\epsilon_{ps}=-4$, 0 , $+4\%$). Figure 6 shows the results obtained, which indicate a well-defined correlation between da/dN and ΔK_{eff} , although some scatter can be observed. The increase of ΔK_{eff} increases da/dN , and a linear trend is obtained. This correlation clearly indicates that plasticity induced crack closure (PICC) is behind the variations of da/dN observed in Figure 4 and therefore behind the effect of pre-strain on FCG.

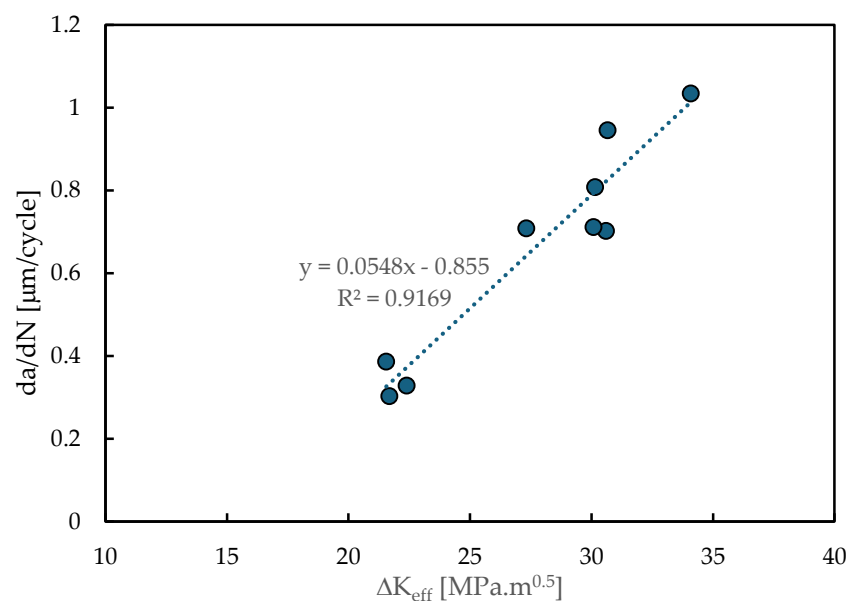


Figure 6. FCG rate versus effective stress intensity factor range for three crack lengths ($a=16.184$; $a=15.048$ mm and $a=15.152$ mm) and three pre-strain conditions ($\epsilon_{ps}=-4$, 0 , $+4\%$). (Plane stress; $R=0.1$; $F_{min}=4.17$ N; $F_{max}=41.67$ N; with contact).

3.2. Influence of Stress Ratio on Pre-Strain Effect

Figure 7 presents results of da/dN versus crack length for a stress ratio $R=0.5$ and different pre-strain values ($\epsilon_{ps}=-4$, 0 , $+4\%$). The dashed lines indicate results obtained for $R=0.1$. The increase of R increased significantly da/dN , which means that the stress ratio has a major impact. The effect of R is usually associated with crack closure phenomenon, therefore the results in Figure 7 indicate that crack closure is affecting the results. The increase of FCG rate with stress ratio has been observed by different authors, namely Mehrzadi e Taheri [38] in a magnesium alloy and Seifi and Hosseini [39] in pure copper.

On the other hand, the effect of pre-strain is less evident for $R=0.5$ than it was for $R=0.1$. Note that linear scales are being used, instead of logarithmic scales. Anyway, the tensile pre-strain produces a slightly higher da/dN for the compressive pre-strain, while the pre-strain $\epsilon_{ps}=0$ has intermediate values. The slope, i.e., the rate of variation of da/dN with crack length, is similar for the different pre-strains. So, there is an inversion of the effects of tensile and compressive pre-strains, relatively to the results obtained for $R=0.1$.

Some oscillations were observed in all curves. In fact, the node release for the simulation of crack growth occurs at minimum load, when the accumulated plastic strain reaches the critical value (110%). Normally this critical value is reached in the middle of a load cycle. So, there is some inaccuracy in the predicted value of N , i.e., the number of load cycles between node release used to calculate da/dN . The problem becomes more relevant when N is relatively small, i.e., when the crack growth rate is relatively high. In this case, although the error is just a fraction of unit, it has some impact on da/dN . These oscillations are a numerical issue, which does not affect the global trend, therefore a smoothing strategy was used to remove them in Figure 7.

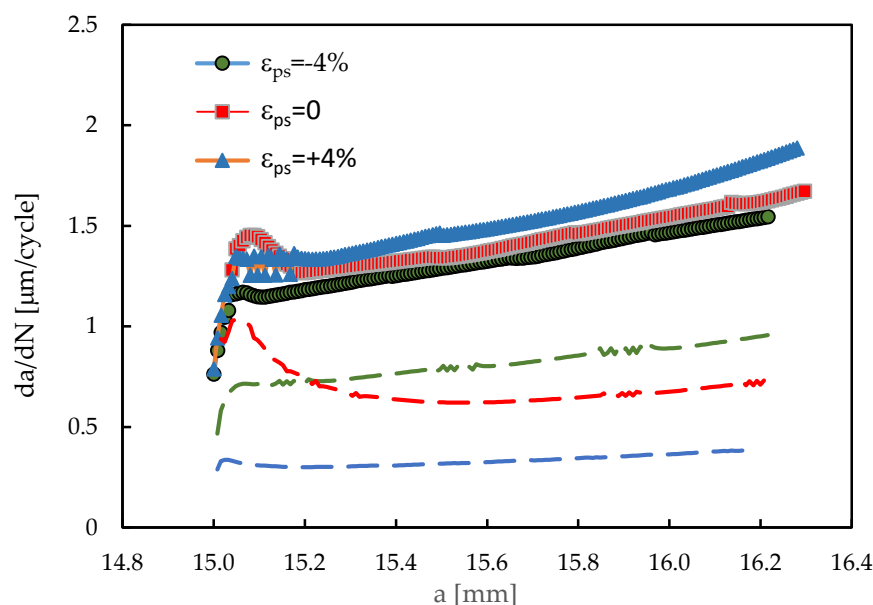


Figure 7. Effect of stress ratio on FCG for different pre-strains (Plane stress; $R=0.5$, $F_{min}=4.17$ N; $F_{max}=41.67$ N; with contact). The dashed lines indicate the results for $R=0.1$.

Figure 8 plots the variation of CTOD with applied load for a stress ratio $R=0.5$ and different pre-strain values ($\epsilon_{ps}=-4$, 0 , $+4\%$). Both the maximum and minimum loads increased relatively to the situation with $R=0.1$, which is represented by the dashed lines. The curves for $R=0.5$ are very similar,

showing a limited effect of pre-strain. The compressive pre-strain presents a slightly lower value of opening load. The comparison with the dashed lines, indicate a great decrease of crack opening level, which has values of U^* in the range 6-11%, while for $R=0.1$ it ranged from 18 to 40%. This reduction of U^* increases the effective load range, which increases significantly the total CTOD range and the elastic and plastic components, δ_e e δ_p , respectively. The variation of U^* also explains the increase of da/dN produced by the increase of R and the reduced effect of pre-strain at $R=0.5$. In fact, since the effect of pre-strain is associated with crack closure, and there is almost no crack closure at $R=0.5$, a minor effect of pre-strain on FCG may be expected.

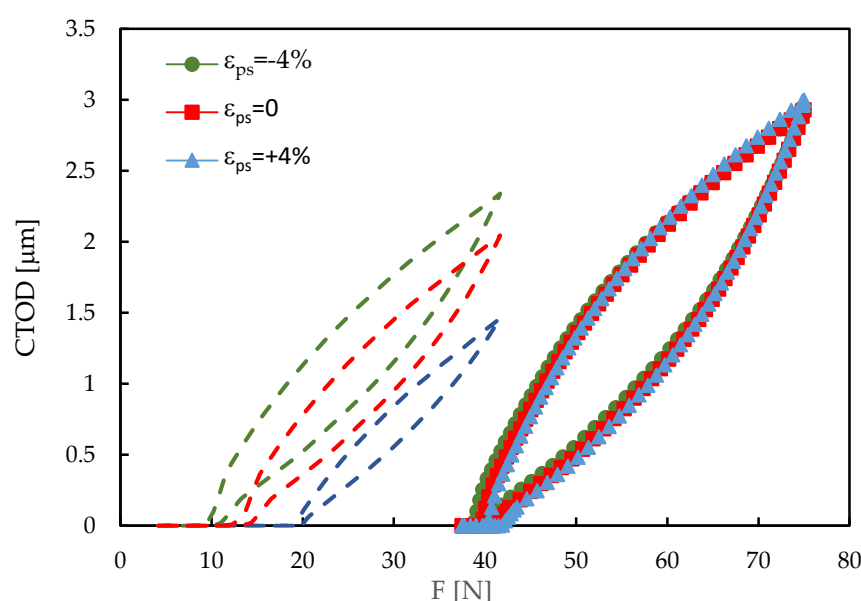


Figure 8. CTOD versus load ($a=16.184$ mm; Plane stress; $F_{min}=37.5$ N; $F_{max}=75$ N; $R=0.5$; with contact). The dashed lines indicate the results for $R=0.1$.

3.3. Effect of Pre-Strain on Variable Amplitude Loading

The influence of pre-strain on the effect of an overload was also studied. The overload was applied at the load cycle number 1500, at a baseline stress ratio $R=0.1$ and considering an overload ratio of 1.5. Figure 9 compares the results of da/dN obtained without pre-strain and with a tensile pre-strain of 4%. These tests took a long time because FCG rate drops significantly after the overload.

The variation of da/dN is according to the typical behaviour observed after an overload [40,41]. Immediately after the overload, there is a sudden increase of da/dN followed by a fast decrease to a minimum value. Some crack extension is required to reach this minimum, which is named delayed retardation. After the minimum there is a progressive increase of FCG rate to the stable value, corresponding to constant amplitude loading. The increase of da/dN is due to crack tip blunting, which eliminates previous crack closure. The variations after blunting are due to the formation of a new residual plastic wake, stronger than that corresponding to constant amplitude loading. In fact, the overload increases the monotonic plastic zone, and this has an impact on crack closure, which is felt after some crack propagation. The two main mechanisms of plasticity induced crack closure are clearly visible in the overloads, i.e., the crack tip blunting and the effect of residual plastic wake.

Comparing the curves for the two pre-strain values ($\epsilon_{ps}=0$, $+4\%$), significant differences are evident. The overload is applied at a shorter crack length for $\epsilon_{ps}=+4\%$ because the crack growth rate is lower while the number of load cycles is the same (1500). Besides, the variations of da/dN are much more pronounced for the case without pre-strain. The extent of propagation affected by the overload is also much higher for $\epsilon_{ps}=0$.

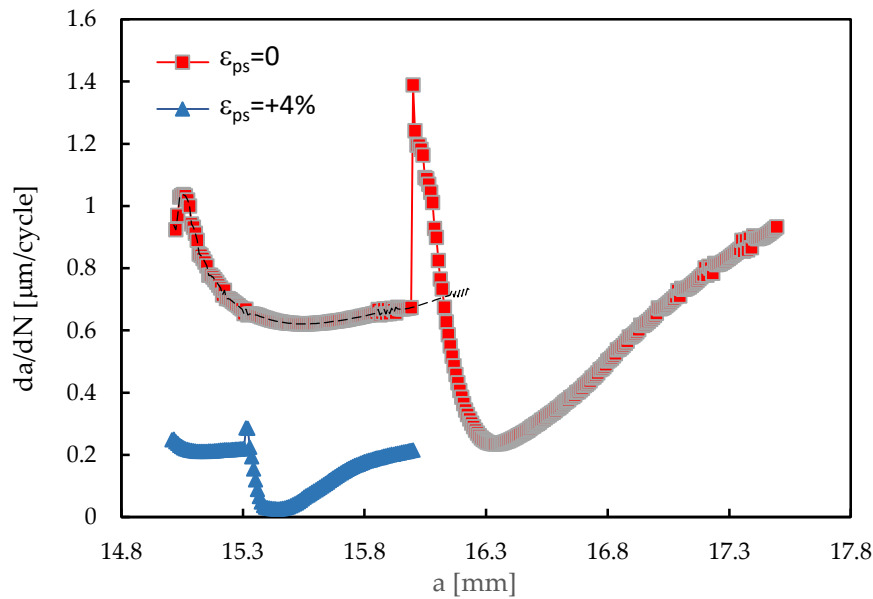
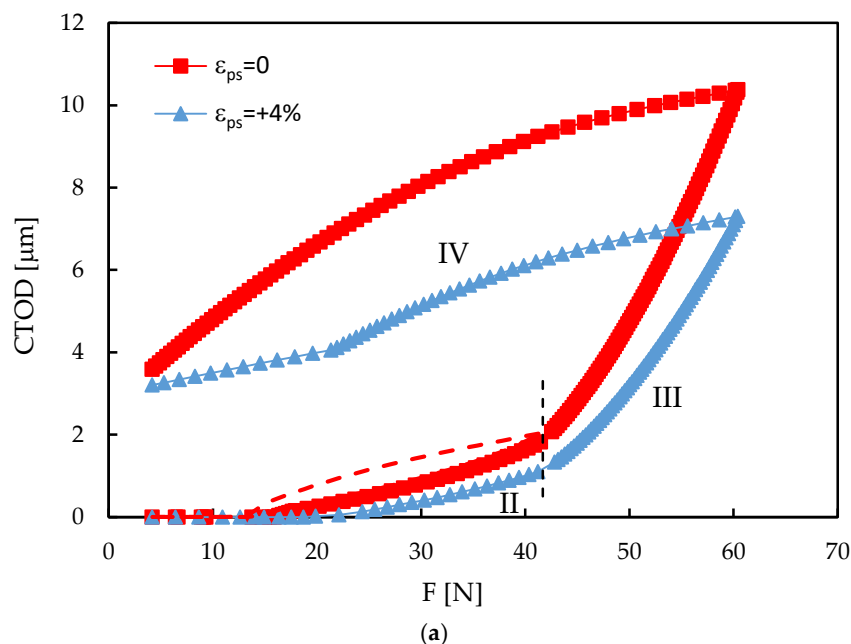


Figure 9. Influence of pre-strain on the effect of overload (OLR=1.5; $F_{OL}=79.17$ N; Plane stress; $F_{min,BL}=4.17$ N; $F_{max,BL}=41.67$ N; $R=0.1$; with contact).

For a better understanding of the effect of pre-strain, Figure 10 plots CTOD curves. Figure 10a presents CTOD variation exactly in the overload cycle. For relatively low loads the crack is closed, i.e., the CTOD is zero. The crack opening occurs first for $\epsilon_{ps}=0$, as already observed in Figure 5. After crack opening, the CTOD increases first linearly and then non-linearly with the load (region II). The linear variation is a result of elastic deformation, while the non-linear variation is due to plastic deformation. The increase of the load above the baseline values, i.e., above $F_{max,BL}=41.67$ N, produces a sudden change of the slope of the curve (region III). The material has not experienced such high loads before, therefore there is a strong plastic deformation, significantly higher than that observed in region II. Consequently, CTOD reaches relatively high values. The subsequent decrease of the load from F_{OL} to F_{min} reduces the blunting (region IV), initially linearly and then non-linearly. The CTOD at the minimum load is the crack tip blunting produced by the overload. The dashed line indicates the behaviour without overload.



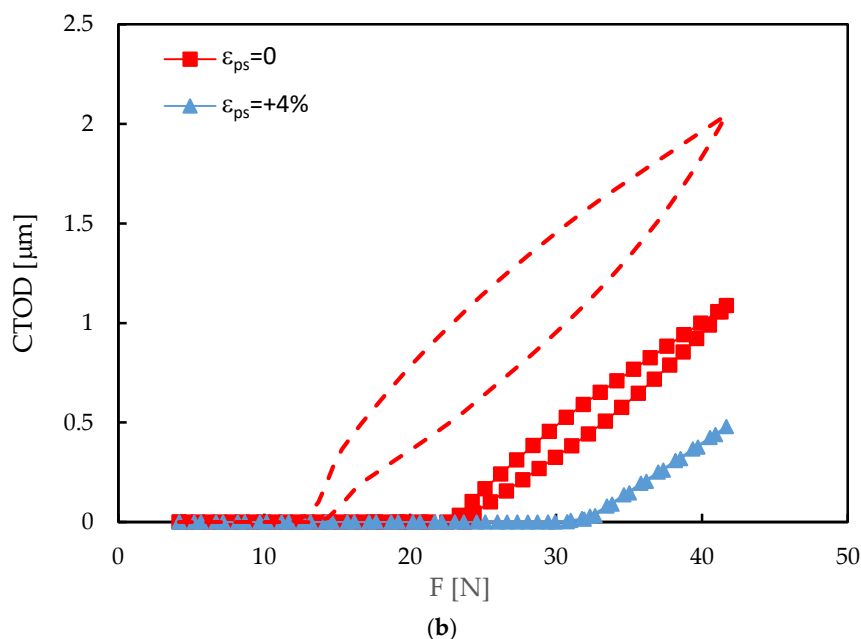


Figure 10. CTOD versus applied load (OLR=1.5; F_{OL} =79.17 N; Plane stress; $F_{min,BL}$ =4.17 N; $F_{max,BL}$ =41.67 N; R =0.1; with contact). (a) Overload cycle. (b) At minimum da/dN (a =16.336 mm and a =15.448 mm for $\epsilon_{ps}=0$ and 4%, respectively). The dashed lines indicate the behaviour without overload.

Figure 10b shows the CTOD curves at the minimum values of da/dN , which occur at crack lengths of 16.336 mm and 15.448 mm for $\epsilon_{ps}=0$ and +4%, respectively. The dashed line indicates the behaviour without overload and without pre-strain. The crack closure is quite relevant, particularly for the tensile pre-strain, much more than observed under constant amplitude loading (Figure 5). $U^*=53.1\%$ for the specimen without pre-strain and $U^*=71.0\%$ for the tensile pre-strain, at the minimum da/dN after the overload. These high values of U^* reduce the effective load range, and therefore the crack tip plastic deformation. This is particularly dramatic for $\epsilon_{ps}=+4\%$, because there is no evidence of plastic CTOD, δ_p . This explains the very small value of da/dN in Figure 9. The slopes of the elastic regimes are very similar, which means that the elastic behaviour is not affected by the overload, as could be expected. Therefore, the minimum da/dN is linked to a peak of crack closure, as was observed by Baptista et al. [42].

4. Discussion

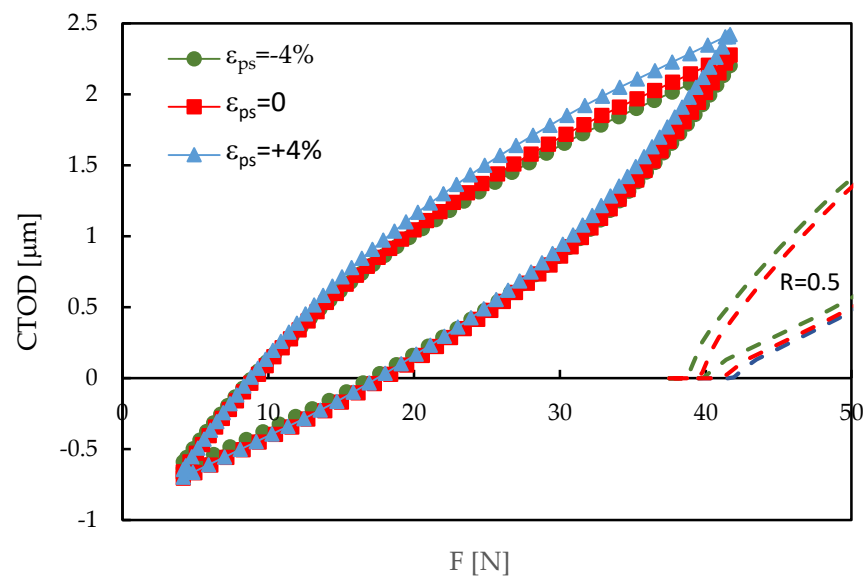
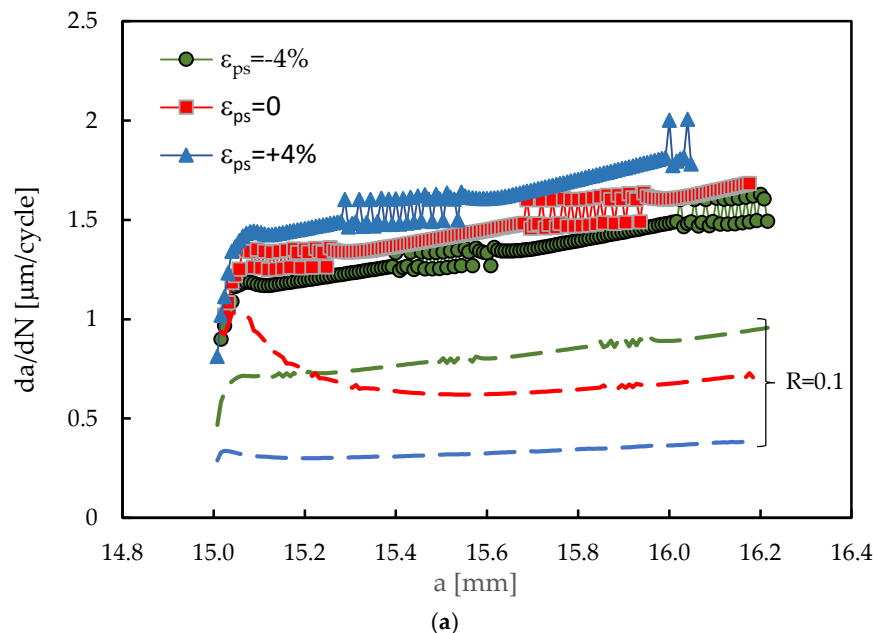
The first issue is the validity of the conclusions obtained using only numerical simulation. Naturally, it would be interesting to have experimental results to validate the numerical predictions. However, this is expensive, since it requires the preparation of specimens with pre-strain and their testing, and time consuming. On the other hand, the present numerical model has already proved to be competent and robust in the simulation of FCG. In fact, the numerical model based on cumulative plastic strain was able to predict the effect of ΔK [37], stress ratio [43], Superblock2020 load pattern [44], overloads [45], load blocks [46], and the effect of lateral holes [47]. These successive validations are also a clear indication that cyclic plastic deformation is the main mechanism responsible for FCG. Besides, numerical approaches are very interesting to develop parametric studies and to analyze the fundamental mechanisms. This is particularly important in the study of the effect of pre-strain, where the mechanisms are not completely understood.

The present results clearly indicate that plasticity induced crack closure is behind the effect of pre-strain. The decrease of ductility is expected to decrease the size of monotonic and reversed plastic zones. This reduces residual plastic deformations and therefore crack closure. On the other hand, there is a decrease of crack blunting which potentiates the effect of residual plastic wake. These mechanisms of opposite effect may explain the different trends observed for different materials, or,

in other words, the dependence on material. Schijve [21] studied AA2024-T3 submitted to a pre-strain of 3%. He also linked the increase of da/dN with crack closure phenomenon.

The material hardening resulting from plastic deformation may also be expected to have a direct effect on crack tip damage. In fact, the cumulative damage will be lower in the hardened material. Therefore, a numerical study was developed without contact of crack flanks, which eliminates crack closure phenomenon from the results. Figure 11a presents da/dN versus crack length. The dashed lines indicate the predictions obtained with contact of crack flanks also for $R=0.1$. As can be seen, there is some effect of pre-strain, but significantly less than observed in the presence of contact of crack flanks. The tensile pre-strain now has a damaging effect, relatively to the situation without pre-strain. On the other hand, the compressive pre-strain reduces da/dN . The numerical oscillations which were eliminated in Figure 7, were not eliminated in here and are now clearly visible.

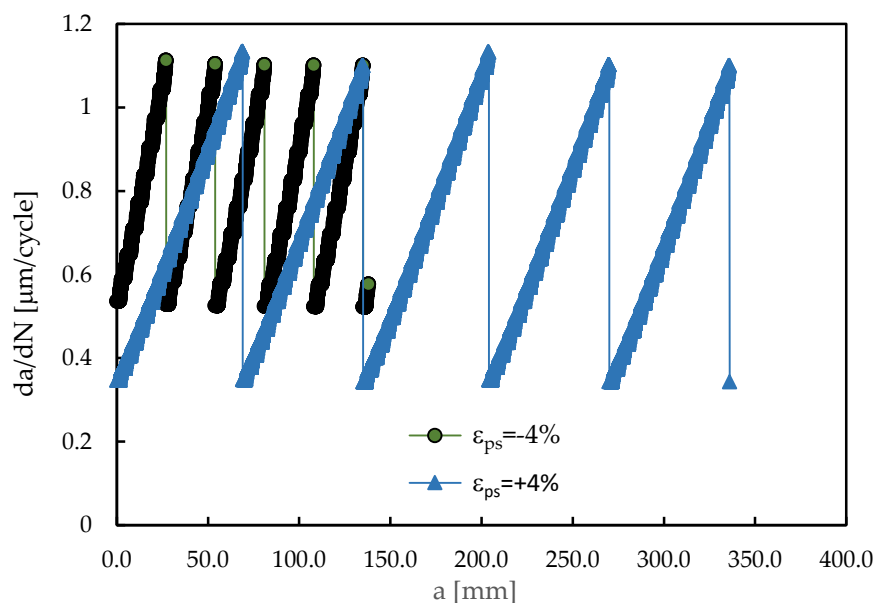
Figure 11b presents the CTOD curves versus load for a crack length $a=16.048$ mm. Negative values of CTOD can be observed, which means that the crack flanks are overlapping. The elimination of the contact is not physically correct, but is particularly interesting to isolate crack tip phenomena, from the influence of crack closure. The applied load range is now totally effective. In other words, the crack tip feels all load cycle without any protection from crack closure phenomenon. This produces an increase of elastic, plastic and total CTOD ranges.



(b)

Figure 11. (a) da/dN versus crack length. (b) CTOD versus load plots at $a=16.048$ mm (Plane stress; $F_{min}=4.17$ N; $F_{max}=41.67$ N; $R=0.1$; without contact).

The inversion of the effect of tensile and compressive pre-strain relatively to the situation with contact (Figure 4) is curious and deserved a closer look. Figure 12 shows the variation of accumulated plastic strain at the crack tip with time (i.e., with load cycling). There are two aspects that deserve special attention: the slope of the curves between node releases and the initial value of plastic strain after node release. The slope represents the rate of accumulation of damage, while the initial value is a consequence of the accumulation of damage in previous positions of crack tip. Figure 12a presents the results obtained for five load increments starting at $a=15.952$ mm, with contact of crack flanks activated. The slopes are clearly different, being higher for the compressive pre-strain. The initial value of accumulated strain is also higher for $\epsilon_{ps}=-4\%$, which indicates larger monotonic and reversed plastic zones. Consequently, assuming 70 load cycles, there are 5 node releases for the compressive pre-strain while the tensile pre-strain only suffers two node releases. These trends are according to the results of Figure 4, i.e., explain the higher da/dN obtained for compressive strain. Figure 12b presents similar results, but without contact of crack flanks. Now, the tensile pre-strain has slightly higher values of initial plastic strain and rate of accumulation of plastic strain. This explains the slightly higher value of da/dN obtained for $\epsilon_{ps}=+4\%$ in Figure 11a.



(a)

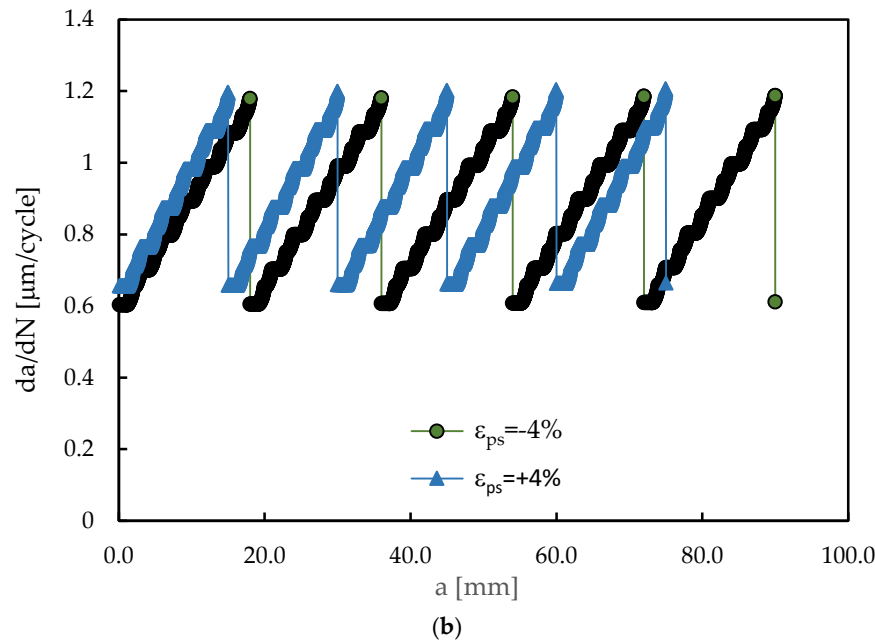


Figure 12. Accumulation of plastic strain at the crack tip with cyclic loading. (a) With contact of crack flanks. (b) Without contact of crack flanks (Plane stress; $F_{min}=4.17$ N; $F_{max}=41.67$ N; $R=0.1$).

5. Conclusions

The main objective here is to study the effect of pre-strain on FCG in AA2024-T351. A numerical model was created to predict FCG assuming that cyclic plastic deformation is the main damage mechanism and using the cumulative plastic strain at the crack tip as driving parameter. Two values of pre-strain were considered: a compressive pre-strain of 4%, a tensile pre-strain of 4%, which were compared with the situation without pre-strain (i.e., $\epsilon_{ps}=-4, 0, +4\%$).

After stabilization of FCG rate, da/dN is higher for the compressive pre-strain, intermediate for the specimen without pre-strain, and lower for the tensile pre-strain. Values of U^* of 18.23, 27.15 and 42.53% were obtained for $\epsilon_{ps}=-4, 0$ and $+4\%$, respectively. The increase of crack opening level decreases the effective load range. A well-defined correlation was obtained between da/dN and ΔK_{eff} for three crack lengths ($a=16.184$; $a=15.048$ mm and $a=15.152$ mm) and the three pre-strain conditions ($\epsilon_{ps}=-4, 0, +4\%$). This clearly indicates that crack closure is explaining the variations of da/dN produced by the pre-strain. The increase of stress ratio from $R=0.1$ to $R=0.5$ reduced significantly the relevance of pre-strain, which is also explained by the reduction of crack closure phenomenon. The effect of pre-strain on da/dN after an overload was also explained by crack closure variations.

Author Contributions: Conceptualization, D.N. and F.A.; methodology, D.N.; formal analysis, A.A. and E.S.; investigation, A.A.; data curation, A.A.; writing—original draft preparation, F.A.; writing—review and editing, D.N. and E.S. All authors have read and agreed to the published version of the manuscript.

Funding: The authors gratefully acknowledge the financial support from the Portuguese Foundation of Science and Technology (FCT) under the projects UIDB/00285/2020 and LA/P/0112/2020. Edmundo Sérgio is also grateful to FCT for the PhD grant with reference 2022.11438.BD.

Data Availability Statement: Dataset available on request from the authors.

Conflicts of Interest: The authors declare no conflicts of interest.

Nomenclature

a	Crack length
a_0	Initial crack length
AA	Aluminium alloy

CA	Constant amplitude
CT	Compact tension
CTOD	Crack tip opening displacement
da/dN	Fatigue crack growth rate
FCG	Fatigue crack growth
F _{max}	Maximum force
F _{min}	Minimum force
F _{open}	Crack opening force
HCF	High-cycle fatigue
LCF	Low-cycle fatigue
OL	Overload
OLR	Overload ratio
R	Stress ratio
UTS	Ultimate tensile strength
U*	Crack opening level
W	Width of CT specimen
ε _{ps}	Pre-strain deformation
ΔK	Range of stress intensity factor

References

1. Hariharan K, Prakash RV. Integrating effect of forming in fatigue life prediction: review of present scenario and challenges. In: Proceedings of the Institution of Mechanical Engineers, Part B: Journal of Engineering Manufacture; 2012. p. 967–79.
2. B. Wang, P. Zhang, Q.Q. Duan, Z.J. Zhang, H.J. Yang, J.C. Pang, Y.Z. Tian, X.W. Li, Z.F. Zhang, High-cycle fatigue properties and damage mechanisms of pre-strained Fe-30Mn-0.9C twinning-induced plasticity steel, Mater. Sci. Eng. A 679 (2017) 258–271, <https://doi.org/10.1016/j.msea.2016.10.043>.
3. Y. Zhou, M. Lin, C. Liu, L. Wang, H. Chen, C. Dan, S. Ma, Z. Chen, H. Wang, Enhancing mechanical properties of uniformly distributed nano TiB₂/2024 Al composite rolling sheet by pre-stretch aging, J. Alloys Compd. 913 (2022) 165172, <https://doi.org/10.1016/j.jallcom.2022.165172>.
4. J. hyun Baek, Y. pyo Kim, C. man Kim, W. sik Kim, C. sung Seok, Effects of pre-strain on the mechanical properties of API 5L X65 pipe, Mater. Sci. Eng. A 527 (2010) 1473–1479. <https://doi.org/10.1016/j.msea.2009.10.017>.
5. A. Mehmanparast, C.M. Davies, D.W. Dean, K. Nikbin, Effects of plastic pre-straining level on the creep deformation, crack initiation and growth behaviour of 316H stainless steel, Int. J. Press. Vessel. Pip. 141 (2016) 1–10. <https://doi.org/10.1016/j.ijpvp.2016.03.013>
6. P. Ghosal, A. Raj, S.K. Paul, Influence of uniaxial and biaxial pre-straining on the low cycle fatigue performance of DP590 steel, Int. J. Fatigue 149 (2021) 106260. <https://doi.org/10.1016/j.ijfatigue.2021.106260>.
7. Puja Ghosal, Surajit Kumar Paul, Abhishek Raj, Influence of uniaxial and biaxial pre-straining on the notch fatigue performance of DP590 steel, Theoretical and Applied Fracture Mechanics 115 (2021) 103072
8. Le Q, Kang HT, Kridli G, Khosrovaneh AK, Yan B. Effect of prestrain paths on mechanical behavior of dual phase sheet steel. Int J Fatigue 2009;31(4):607–15.
9. Fredriksson K, Melander A, Hedman M. Influence of prestraining and ageing on fatigue properties of high-strength sheet steels. Int J Fatigue 1988;10(3):139–51.
10. Wang B, Zhang P, Duan QQ, Zhang ZJ, Yang HJ, Pang JC, et al. High-cycle fatigue properties and damage mechanisms of pre-strained Fe-30Mn-0.9 C twinning-induced plasticity steel. Mater Sci Eng, A 2017;679:258–71.
11. Walker J, Thomas DJ, Gao Y. Effects of shot peening and pre-strain on the fatigue life of dual phase Martensitic and Bainitic steels. J Manuf Processes 2017;26: 419–24.
12. Ji D, Zhang M, Zhu D, Luo S, Li L. Influence of microstructure and pre-straining on the bake hardening response for ferrite-martensite dual-phase steels of different grades. Mater Sci Eng, A 2017;708:129–41.
13. Wu H, Hamada S, Noguchi H. Pre-strain effect on fatigue strength characteristics of SUH660 plain specimens. Int J Fatigue 2013;55:291–8.

14. Froustey C, Lataillade JL. Influence of large pre-straining of aluminium alloys on their residual fatigue resistance. *Int J Fatigue* 2008;30:908–16. <https://doi.org/10.1016/j.ijfatigue.2007.06.011>.
15. Le Roux, J. C., Taheri, S., Sermage, J. P., Colin, J., & Fatemi, A. (2008, January). Cyclic deformation and fatigue behaviors of stainless steel 304L including mean stress and pre-straining effects. In *ASME Pressure Vessels and Piping Conference*, (Vol. 48265, pp. 411-420).
16. Gustavsson A, Melander A. Variable-amplitude fatigue of a dual-phase sheet steel subjected to prestrain. *Int J Fatigue* 1994;16(7):503–9.
17. Parker TE, Montgomery GL. Effect of Balanced Biaxial Stretching on the Low Cycle Fatigue Behavior of SAE 1008 Hot Rolled Low Carbon Steel. *SAE Trans* 1975: 308–18.
18. Das B, Singh A, Paul SK. Low cycle fatigue performance of DP600 steel under various pre-straining paths. *Int J Fatigue* 2020;132:105331.
19. AV Rex , S K Paul, A Singh, The influence of equi-biaxial and uniaxial tensile pre-strain on the low cycle fatigue performance of the AA2024-T4 aluminium alloy, *International Journal of Fatigue* 173 (2023) 107699.
20. R. Branco, J.D. Costa, L.P. Borrego, S.C. Wu, X.Y. Long, F.V. Antunes, Effect of tensile pre-strain on low-cycle fatigue behaviour of 7050-T6 aluminium alloy, *Engineering Failure Analysis* 114, 2020, 104592. <https://doi.org/10.1016/j.engfailanal.2020.104592>
21. J. Schijve, THE EFFECT OF PRE-STRAIN ON FATIGUE CRACK GROWTH AND CRACK CLOSURE, *Engineering Fracture Mechanics*, 8, Issue 4, 1976, Pages 575-581.
22. Kassim S. Al-Rubaie, Emerson K.L. Barroso, Leonardo B. Godefroid, Fatigue crack growth analysis of pre-strained 7475-T7351 aluminum alloy, *International Journal of Fatigue* 28 (2006) 934–942. [10.1016/j.ijfatigue.2005.09.008](https://doi.org/10.1016/j.ijfatigue.2005.09.008)
23. Satya Anandavijayan, Ali Mehmanparast, Jarryd Braithwaite, Feargal Brennan, Amir Chahardehi, Material pre-straining effects on fatigue behaviour of S355 structural steel, *Journal of Constructional Steel Research* 183 (2021) 106707. <https://doi.org/10.1016/j.jcsr.2021.106707>
24. Tai Shan Kang, H.W. Liu, The effect of pre-stress cycles on fatigue crack growth-an analysis of crack growth mechanism, *Eng. Fract. Mech.* 6 (1974) 631–638. [https://doi.org/10.1016/0013-7944\(74\)90062-9](https://doi.org/10.1016/0013-7944(74)90062-9).
25. J. Wasen, K. Hamberg, B. Karlsson, The influence of prestrain and ageing on fatigue crack growth in a Dual-Phase Steel, *Scr. Metall.* 18 (1984) 621–624.
26. P.R. Arora, M.R. Raghavan, Y.V.R.K. Prasad, Effect of prestrain on fatigue crack propagation in mild steel containing non-metallic inclusions, *Eng. Fract. Mech.* 29 (1988) 67–79. [https://doi.org/10.1016/0013-7944\(88\)90007-0](https://doi.org/10.1016/0013-7944(88)90007-0).
27. V.M. Radhakrishnan, P.S. Baburamani, An investigation of the effect of pre-straining on fatigue crack growth, *Mater. Sci. Eng.* 17 (1975) 283–288. [https://doi.org/10.1016/0025-5416\(75\)90237-2](https://doi.org/10.1016/0025-5416(75)90237-2).
28. S. Kim, T. Song, H. Sung, S. Kim, Effect of Pre-Straining on High Cycle Fatigue and Fatigue Crack Propagation Behaviors of Precipitation Hardened Steel, *Met. Mater. Int.* 27 (2021) 1383–1391. <https://doi.org/10.1007/s12540-019-00436-7>.
29. T. Leitner, G. Trummer, R. Pippan, A. Hohenwarther, Influence of severe plastic deformation and specimen orientation on the fatigue crack propagation behavior of a pearlitic steel, *Mater. Sci. Eng. A* 710 (2018) 260–270. <https://doi.org/10.1016/j.msea.2017.10.040>.
31. Ashkenazi D. How aluminum changed the world: A metallurgical revolution through technological and cultural perspectives. *Technol Forecast Soc Change* 2019;143:101–13.
32. Zhang X, Chen Y, Hu J. Recent advances in the development of aerospace materials. *Prog Aerosp Sci* 2018;97:22–34. <https://doi.org/10.1016/j.paerosci.2018.01.001>.
33. Dursun T, Soutis C. Recent developments in advanced aircraft aluminium alloys. *Mater Des* 2014;56:862–71.
34. Swift, H.W. Plastic instability under plane stress. *J Mech Phys Solids* 1952, 1, 1–18. [https://doi.org/10.1016/0022-5096\(52\)90002-1](https://doi.org/10.1016/0022-5096(52)90002-1).
35. Lemaitre J, Chaboche JL. *Mechanics of Solids Materials*. Cambridge University Press, Cambridge, 1985.
36. MF Borges; P Lopez-Crespo, FV Antunes; B Moreno; P Prates; D Camas; DM Neto, Fatigue crack propagation analysis in 2024-T351 aluminium alloy using nonlinear parameters, *Int J Fatigue* 153 (2021) 106478. <https://doi.org/10.1016/j.ijfatigue.2021.106478>

37. L.F. Menezes, C. Teodosiu, Three-dimensional numerical simulation of the deep drawing process using solid finite elements, *J Mater Proc Technol* 97 (2000) 100–106.
38. MF Borges, DM Neto, FV Antunes, Numerical simulation of fatigue crack growth based on accumulated plastic strain, *Theoretical and Applied Fracture Mechanics* 108 (2020) 102676 <https://doi.org/10.1016/j.tafmec.2020.102676>
39. M. Mehrzadi and F. Taheri, "The influence of negative and positive stress ratios on crack growth rate in AM60B magnesium alloy," *Materials Science and Engineering: A*, vol. 545, pp. 68–77, May 2012, doi: 10.1016/J.MSEA.2012.02.091.
40. R. Seifi and R. Hosseini, "Experimental study of fatigue crack growth in raw and annealed pure copper with considering cyclic plastic effects," *Theoretical and Applied Fracture Mechanics*, vol. 94, pp. 1–9, Apr. 2018, doi: 10.1016/J.TAFMEC.2017.12.003
41. L. P. Borrego, J. M. Ferreira, and J. M. Costa, "Fatigue crack growth and crack closure in an AlMgSi alloy," *Fatigue Fract Eng Mater Struct*, vol. 24, no. 4, pp. 255–265, Apr. 2001, doi: 10.1046/J.1460-2695.2001.00383.X.
42. S. Zheng, Q. Yu, Z. Gao, and Y. Jiang, "Loading history effect on fatigue crack growth of extruded AZ31B magnesium alloy," *Eng Fract Mech*, vol. 114, pp. 42–54, Dec. 2013, doi: 10.1016/J.ENGFRACMECH.2013.10.012.
43. JB Baptista, FV Antunes, L Correia, R Branco, A numerical study of the effect of single overloads on plasticity induced, *Theoretical and Applied Fracture Mechanics* 88 (2017) 51–63. <http://dx.doi.org/10.1016/j.tafmec.2016.12.001>
44. Neto DM, Borges MF, Antunes FV. Mechanisms of fatigue crack growth in single overloads. *Theor Appl Fract Mech* 2021;114:103024. <https://doi.org/10.1016/j.tafmec.2021.103024>
45. Neto DM, Borges MF, Antunes FV, Sunder R. Numerical analysis of SuperBlock2020 loading sequence. *Engng Fract Mech* 2022;260:108178. <https://doi.org/10.1016/j.engfracmech.2021.108178>
46. D.M. Neto, J. Pedro, M.F. Borges, L.F.P. Borrego, E.R. Sérgio, FV Antunes, Numerical prediction of fatigue crack growth based on cumulative plastic strain versus experimental results for AA6082-T6, *Int J Fract* 240, 167–181 (2023) <https://doi.org/10.1007/s10704-022-00680-w>
47. D.M. Neto, E.R. Sérgio, M.F. Borges, L.P. Borrego, F.V. Antunes, Effect of load blocks on fatigue crack growth, *International Journal of Fatigue* 162 (2022) 107001. <https://doi.org/10.1016/j.ijfatigue.2022.107001>
48. D.M. Neto, N. Cavaleiro, E.R. Sérgio, J. Jesus, A. Camacho-Reyes, F.V. Antunes, Effect of crack flank holes on fatigue crack growth. *International Journal of Fatigue* 2023, 170, 107505. <https://doi.org/10.1016/j.ijfatigue.2023.107505>
49. M.S. Rana, C. Makabe, G. Fujiwara, The effect of hole shape on the extent of fatigue life improvement by cold expansions, *Eng Fail Anal.* 16(2009)2081-2090, <https://doi.org/10.1016/j.engfailanal.2009.02.001>.
50. T.N. Chakherlou, M. Shakouri, A.B. Aghdam, A. Akbari, Effect of cold expansion on the fatigue life of Al 2024-T3 in double shear lap joints : Experimental and numerical investigations, *Mater Des.* 33(2012)185-196, <https://doi.org/10.1016/j.matdes.2011.07.024>.
51. Z. Semari, A. Aid, A. Benhamena, A. Amrouche, M. Benguediab, A. Sadok, N. Benseddq, Effect of residual stresses induced by cold expansion on the crack growth in 6082 aluminum alloy, *Eng Fract Mech.* 99(2013)159-168, <https://doi.org/10.1016/j.engfracmech.2012.12.003>.
52. H.D. Gopalakrishna, H.N.N. Murthy, M. Krishna, M.S. Vinod, A.V. Suresh, Cold expansion of holes and resulting fatigue life enhancement and residual stresses in Al 2024 T3 alloy - An experimental study, *Eng Fail Anal.* 17(2010)361-368, <https://doi.org/10.1016/j.engfailanal.2009.08.002>.
53. Radhakrishnan VM, Baburamani PS. Initiation and propagation of fatigue crack in pre-strained material [J]. *International Journal of Fracture.* 1976,
54. Li HF, Wang ZB, Sun XJ, Qian CF. Experimental investigation of the strain-strengthen effect on the existed I+II mixed mode fatigue crack transformation propagation in an austenite stainless steel [C]. In: *Proceedings of the ASME 2013 Pressure Vessels & Piping Division Conference.* 2013, 7: 14-18.

Disclaimer/Publisher's Note: The statements, opinions and data contained in all publications are solely those of the individual author(s) and contributor(s) and not of MDPI and/or the editor(s). MDPI and/or the editor(s)

disclaim responsibility for any injury to people or property resulting from any ideas, methods, instructions or products referred to in the content.